

ENHANCED ADVANCING FRONT TECHNIQUES FOR MESH GENERATION
IN RADIATIVE HEAT TRANSFER PROBLEM

ZURAIDA ABAL ABAS

UNIVERSITI TEKNOLOGI MALAYSIA

ENHANCED ADVANCING FRONT TECHNIQUES FOR MESH GENERATION
IN RADIATIVE HEAT TRANSFER PROBLEM

ZURaida BINTI ABAL ABAS

A thesis submitted in fulfilment
of the requirements for the award of the degree of
Doctor of Philosophy (Mathematics)

Faculty of Science
Universiti Teknologi Malaysia

MARCH 2012

To my husband, parents and family

– thank you for everything

ACKNOWLEDGEMENT

So many people have played a significant role in my life as I entered the world of PhD student. I would like to thank my supervisor, Prof Dr. Shaharuddin Salleh who has always provided ideas, guidance and motivation as well as his assistance throughout this work. Special thanks to my other supervisor, Prof Dr. Zainuddin Abd Manan who introduced me the concept of ethylene furnace.

I also would like to thank the staff of Unit Cuti Belajar as well as Universiti Teknikal Malaysia Melaka and Kementerian Pengajian Tinggi for providing support and financial assistance during my study. Special thanks to Prof Dr Shahrin Sahib for his support and Dr. Simon Botley for providing language assistance. Same thing goes to all my friends who have always shared the up and down of PhD study.

Finally, I would not able to complete my study without the support and prayers from my husband, Mas Hariadi Mohamed, my son Ahmad Aqhil Bikhair and both my mother and my mother in law. To Allah, the Lord Almighty, thank you for the greatest guidance, assistance and each and everything.

ABSTRACT

Mesh generation is a mathematical technique to produce meshes in the form of triangle and rectangles on a given domain for approximating values such as heat, temperature and pressure. The values are approximated using numerical methods such as finite element, finite difference and finite volume based on some given boundary conditions. In our work, a conceptual model has been designed for allowing a set of sensors to be deployed along the wall of an ethylene cracker furnace. The main function for the deployment is to provide input in the form of boundary values for approximating the temperatures of flue gas and the radiative heat flux distribution inside the furnace. New models called Enhanced Advancing Front Techniques (EAFT) have been proposed which improve on the existing standard advancing front in the form of element creation procedure, internal gradation control as well as the post-processing procedure for mesh quality improvement. EAFT is applied to discretise the domain of the conceptual model of the ethylene furnace with the requirements of having the location of sensors deployed along the wall as boundary nodes as well as forming boundary elements, generating nodes at a certain boundary with linearly different lengths of boundary edges using layer concept as interior gradation controls and constructing the triangular element directly in every iteration without having to re-order the front or delete the existing elements. The quality of the initial mesh is determined using the normalized measure of skewness provided by the GAMBIT software. The final mesh is obtained once the post-processing procedure of improving the mesh quality has been applied to the initial mesh. EAFT provides the framework for the heat to be approximated using the discrete ordinate method, which is a variant of the finite volume method. Simulation results produced using FLUENT support our findings for effectively approximating the flue gas temperature distribution, the circumferential radiative heat flux incident at the reactor coils as well as the circumferential reactor coil temperature in the conceptual model of ethylene furnace at the end of the study.

ABSTRAK

Generasi jaringan adalah satu teknik matematik untuk menghasilkan jejaring dalam bentuk segi tiga dan segi empat pada domain atau ruang tertentu bagi mendapatkan nilai anggaran seperti haba, suhu dan tekanan. Nilai anggaran didapati dengan menggunakan kaedah berangka seperti unsur terhingga, beza terhingga dan isipadu terhingga berdasarkan kepada beberapa syarat sempadan yang diberikan. Dalam kerja ini, model konsep telah direka untuk membolehkan satu set sensor yang akan digunakan di sepanjang dinding relau etilena. Fungsi utama sensor tersebut adalah untuk memberi input dalam bentuk nilai-nilai sempadan bagi mendapatkan nilai anggaran suhu gas serombong dan fluks sinaran haba di dalam relau. Model baru yang dipanggil *Enhanced Advancing Front Technique* (EAFT) telah dicadangkan untuk memperbaiki kaedah memajukan depan sedia ada dari segi prosedur penghasilan elemen, kawalan penggredan dalaman serta prosedur selepas pemrosesan untuk meningkatkan kualiti jejaring. EAFT digunakan untuk membahagikan ruang model konsep relau etilena dengan memenuhi keperluan berikut; lokasi sensor yang di letakan di sepanjang dinding sebagai nod sempadan serta membentuk elemen sempadan, menjana nod di sempadan tertentu dengan jarak linear yang berbeza pada sempadan menggunakan konsep lapisan sebagai kawalan penggredan dalaman dan membina elemen segi tiga secara langsung dalam setiap lelaran tanpa menyusun semula depan atau memadam elemen-elemen yang sedia ada. Kualiti jejaring awal ditentukan dengan menggunakan ukuran kepencongan normal yang disediakan oleh perisian GAMBIT. Jejaring akhir diperolehi sebaik sahaja prosedur pemrosesan akhir untuk memperbaiki kualiti jejaring awal telah digunakan. EAFT menyediakan rangka kerja bagi menganggarkan suhu dan haba menggunakan kaedah ordinat diskret, yang merupakan varian kepada kaedah isipadu terhingga. Keputusan simulasi yang dihasilkan dengan menggunakan FLUENT menyokong penemuan kami untuk mendapatkan taburan suhu gas serombong, fluks haba sinaran pada lilitan gegelung reaktor serta suhu lilitan gegelung reaktor dalam model konsep relau etilena pada akhir kajian.

TABLE OF CONTENTS

CHAPTER	TITLE	PAGE
	TITLE PAGE	i
	DECLARATION	ii
	DEDICATION	iii
	ACKNOWLEDGEMENT	iv
	ABSTRACT	v
	ABSTRAK	vi
	TABLE OF CONTENTS	vii
	LIST OF TABLES	xi
	LIST OF FIGURES	xiii
	LIST OF SYMBOLS / NOTATIONS	xxvi
1	INTRODUCTION	
	1.1 Research Background	1
	1.2 Problem Statement	3
	1.3 Objective and Scope of the Research	4
	1.4 Research Methodology	5
	1.5 Significance of the Research	9
	1.6 Outlines of the Thesis	10
2	LITERATURE REVIEW	
	2.1 Introduction	13
	2.2 The Ethylene Furnace and its Overview of the	

	Process	14
2.3	The Phenomena of Heat Transfer in Ethylene Furnace and the Current Technique of Monitoring Heat Transfer Parameter	18
2.4	Mesh Triangulation	19
2.5	The General Basic Step of the Standard Advancing Front Technique (SAFT)	21
2.6	Recent Approaches in Advancing Front Technique	25
2.7	Mesh Quality Improvement	31
2.8	The Concept of Radiation	33
2.9	The Discrete Ordinate Method (DOM)	35
2.10	The Sensor for High Temperature	37
3	THE ENHANCED ADVANCING FRONT TECHNIQUE -1	
3.1	Introduction	40
3.2	The Condition of Invalid or Undecided Element Creation	41
3.3	The Extension of a Normal Case in the SAFT for Triangular Element Creation	43
3.4	The Implementation of Element Creation Procedure Based on Five Cases of EAFT-1 in AutoCAD LT	48
3.5	The Mathematical Equations Behind the Work of EAFT-1 in AutoCAD	66
3.6	The Significance of Incorporating Extension Cases to the Standard Algorithm of the Advancing Front Technique	68
3.7	The Simulation Results	68
4	THE ENHANCED ADVANCING FRONT TECHNIQUE-2	
4.1	Introduction	78

4.2	The Problem Statement and the Simplified Version of the Conceptual Model	79
4.3	The Enhanced Advancing Front Technique-2 (EAFT-2) Algorithm	81
4.3.1	The Layer Concept and its Significance to the EAFT-2	83
4.3.2	The General Idea of the Enhanced Advancing Front Technique-2 (EAFT-2)	85
4.3.3	The Six Cases of Consideration for Element Creation Procedure	87
4.3.4	The Implementation of Element Creation Procedure Based on Six Cases of EAFT-2 In AutoCAD LT	92
4.3.5	The Mathematical Equations Behind the Work of EAFT-2 in AutoCAD	108
4.3.6	The Entire Front Starting with the Shortest Edge as the Departure Zone	108
4.3.5	The Significance of EAFT-2	115
4.4	The Integration of the Value from the Sensors and the Unstructured Mesh with the Governing Equation of Radiative Heat Transfer	116
4.5	The difference between SAFT and EAFT-2	117
4.6	The Simulation Result	118

5

THE ENHANCED ADVANCING FRONT TECHNIQUE-3

5.1	Introduction	129
5.2	The Conceptual Model	130
5.3	The Enhanced Advancing Front Technique-3 Algorithm	131
5.3.1	The General Idea of the Enhanced Advancing Front Technique-3 (EAFT-3)	133
5.3.2	The Seven Cases of Consideration for	

	Element Creation Procedure	135
5.3.3	The Implementation of Element Creation Procedure Based on Seven Cases of EAFT-3 In AutoCAD LT	140
5.3.4	The Mathematical Equations Behind the Work of EAFT-3 in AutoCAD	162
5.3.5	The Departure Zone in EAFT-3 for the Element Creation Procedure	163
5.3.6	The Newly Created Post-processing Procedure	170
5.3.5	The Significance of EAFT-3	171
5.4	The Difference Between SAFT and EAFT-3	172
5.5	The Simulation Result	173
6	CONCLUSION	185
	REFERENCES	190
	LIST OF PUBLICATIONS	196

LIST OF TABLES

TABLE NO.	TITLE	PAGE
2.1	The configuration of ethylene furnace taken from [33]	15
3.1	The relationship between Q_{EAS} and mesh quality together with the total elements in the range respectively for initial unstructured grids generated with EAFT-1 for the domain as in Figure 3.15.	71
3.2	The relationship between Q_{EVS} and mesh quality together with the total elements in the range respectively for unstructured grids generated with EAFT-1 for the domain as in Figure 3.15	73
3.3	The relationship between Q_{EAS} and mesh quality together with the total elements in the range respectively for unstructured grids generated with EAFT-1 for the domain as in Figure 3.18	75
3.4	The relationship between Q_{EVS} and mesh quality together with the total elements in the range respectively for unstructured grids generated with EAFT-1 for the domain as in Figure 3.18	76
4.1	The result for the layer concept for Figure 4.3b	84
4.2	The relationship between Q_{EAS} and mesh quality together with the total elements in the range respectively for unstructured grids generated with EAFT-2 for the domain of one circle as in Figure 4.19	122
4.3	The relationship between Q_{EAS} and mesh quality together with the total elements in the range respectively for unstructured grids generated with EAFT-2 for the domain of two circles as in Figure 4.21	124
5.1	The number of elements in percentages with respect to the range of the quality of the initial unstructured mesh generated with EAFT-3 for the conceptual model of ethylene furnace.	177

5.2	The number of elements in percentages with respect to the range of the quality of the initial unstructured mesh generated with SAFT in GAMBIT for the conceptual model of ethylene furnace	178
5.3	The number of elements in percentages with respect to the range of the quality of the final unstructured mesh generated with EAFT-3 for the conceptual model of ethylene furnace	180
5.4	The mesh quality of initial unstructured mesh for the simplified conceptual model with one circle by using algorithm of EAFT-2 and EAFT-3	182

LIST OF FIGURES

FIGURE NO.	TITLE	PAGE
1.1a	The framework of the research – part 1	8
1.1b	The framework of the research – part 2	9
2.1	The ethylene furnace plant taken from [49]	14
2.2	The illustration of radiant section or firebox in ethylene furnace taken from [33]	15
2.3	The interaction of the processes in the ethylene furnace	17
2.4a	Elements that satisfy the circumcircle property.	20
2.4b	Elements that do not satisfy the circumcircle property.	20
2.5a	Detection of the elements which contain the new inserted point.	20
2.5b	The creation of new elements by connecting the new point to the points at the boundary of the convex cavity.	20
2.6	The illustration for the incremental point insertion strategy.	21
2.7a	A two dimensional domain with connected boundary curves	22
2.7b	A set of edges forming initial front and the background grid consists of triangle ABC and ADC	22
2.8	The illustration of element with regards to front, taken from [68]	23
2.9a	The selected edge (a,b) and the position of IP	23
2.9b	A circle is constructed with centre at IP and the radius of the circle following the empirical rule	23
2.10	The illustration of the front ‘marching’ process into the interior of the domain, taken from [71]	25

2.11	The general scheme of SAFT	25
2.12	The determination of optimal number of points taken from [75]	26
2.13	The first local umbrella at the left and the extremely right is completing two local umbrella [76]	27
2.14	Choosing the correct segment at point p [76]	27
2.15a	The first element is generated by connecting the centre of the circle and become the initial front, taken from [77]	28
2.15b	The second element is generated by adding a new circle and connect the centre of the circle to the existing element, taken from [77]	28
2.16a	The packing of circles with random size across the domain, taken from [77]	28
2.16b	The resulted unstructured mesh with random size, taken from [77]	28
2.17	The mesh/grid generation algorithm taken from [78]	29
2.18	The latest approach and advancement for advancing front technique in terms of element construction	30
2.19	Diagonal swapping	32
2.20	The shift for the interior node	32
2.21	The radiative heat transfer in Cartesian coordinate system taken from [88]	34
2.22	Cell centred control volume in 2D unstructured mesh, taken from [88]	36
2.23	A thermocouple made from iron and constantan wire taken from [90]	38
2.24	A typical RTD sensor taken from [95]	38
2.25	A variety of sizes and shapes of thermistors taken from [97]	39
3.1a	Definition of boundary edges at boundary curves	42
3.1b	Edge (7,9) as the base edge. The IP is out of the boundary and no points lie within the circle	42

3.2	The second problem where the base edge is (a,b) and it cannot connect to the IP directly	42
3.3a	No objects lie within the circle	44
3.3b	An equilateral triangle is constructed	44
3.4a	Two types of object lie within the circle which are active nodes and edges	45
3.4b	Node d is selected as the vertex	45
3.5a	An active edge intersected with the circle and $L_{p_1p_2} < r$	46
3.5b	The IP becomes the new active node d for the triangular element	46
3.6a	The intersected active edge is (b,c) and $L_{p_1p_2} \geq r$	47
3.6b	The triangular element is constructed by connecting the node associated with the intersected active edge with the base edge	47
3.7	The general scheme of EAFT-1	47
3.8	The object snap mode in drafting setting	48
3.9a	The computational domain	49
3.9b	The background mesh consists of triangle ABD and BCD	49
3.9c	A set of nodes are placed by using command multiple points	50
3.9d	The crosshair is positioned at the initial node until the small purple color circle appears at the node	51
3.9e	The crosshair is moved towards the end node until the small purple colored circle appears at the respective node	51
3.9f	The line which represents boundary edge is automatically created where it connects the initial node and end node	52
3.9g	A set of boundary edges	52
3.10a	Active edge considered for example 1 is (a,b)	54
3.10b	The selection of circle drawing tool	54
3.10c	The crosshair is moved towards node b until a small purple colored circle appears at the node	55

3.10d	A circle with its centre at node a and radius equal to the length of the active edge is created	55
3.10e	A circle with its centre at node b and radius equal to the length of the active edge is created	56
3.10f	A command to create single point is selected	56
3.10g	The crosshair is moved towards the point where the circles intersect until small purple colored x appear at the intersection	57
3.10h	The intersection of the two circles is selected as the IP and the previous two circles are deleted	57
3.10i	A circle for example 1 with its centre at IP and radius obtained from empirical rule	58
3.10j	An equilateral triangle is constructed for example 1	59
3.11a	Active edge considered for example 2 is (a,b) and a circle is constructed for example 2	60
3.11b	Node c is selected as a vertex for example 2	61
3.12a	Active edge considered for example 3 is (a,b) and a circle is constructed	62
3.12b	Intersection points marked as point $p1$ and $p2$	63
3.12c	Node c is selected to be the vertex to form the triangle element for example 3	63
3.13a	Active edge considered for example 5 is (a,b) and a circle is constructed	64
3.13b	The intersection points $p1$ and $p2$ and its distance	65
3.13c	Equilateral triangle is created when IP is selected and becomes node e for example 4	66
3.14a	A domain with background grid consists of triangle ABD and ADC	68
3.14b	A set of boundary edges	68
3.15	The resulted initial unstructured triangular mesh using EAFT-1	69
3.16a	Element with quality $Q_{EAS} = 0$	70

3.16b	Element with quality $0 < Q_{EAS} \leq 0.25$	70
3.16c	Element with quality $0.25 < Q_{EAS} \leq 0.5$	71
3.16d	Element with quality $0.5 < Q_{EAS} \leq 0.75$	71
3.17a	Element with quality $Q_{EVS} = 0$	72
3.17b	Element with quality $0 < Q_{EVS} \leq 0.25$	72
3.17c	Element with quality $0.25 < Q_{EVS} \leq 0.5$	72
3.17d	Element with quality $0.5 < Q_{EVS} \leq 0.75$	72
3.18	The resulting unstructured mesh at the end of mesh smoothing procedure	74
3.19a	Element with quality $Q_{EAS} = 0$	74
3.19b	Element with quality $0 < Q_{EAS} \leq 0.25$	74
3.19c	Element with quality $0.25 < Q_{EAS} \leq 0.5$	75
3.20a	Element with quality $Q_{EVS} = 0$	76
3.20b	Element with quality $0 < Q_{EVS} \leq 0.25$	76
3.21	The contour of temperature distribution of the flue gas	77
3.22	The plot of convergence for the simulation	77
4.1a	A simplified problem domain for the initial study with only 1 circle representing half a reactor coil	80
4.1b	A simplified problem domain for the initial study with two circles representing 1 complete reactor coil	80
4.2a	Definition of boundary edges at boundary curves	82
4.2b	The whole domain is divided into sub-regions	83
4.3a	A straight line AB before applying layer concept	84
4.3b	A set of nodes are placed at the line segments produced by employing layer concept at line AB	84

4.4	Applying the layer concept at the newly created line segment (the newly created boundary of the sub-regions- AB, CD, EF and GH)	85
4.5a	(11,12) is selected as the base edge for element construction	86
4.5b	A triangular element is constructed with (11,12) as the base edge	86
4.6a	Intersection point of the circle is the IP. Base edge is (a,b)	86
4.6b	IP on the perpendicular bisector of the base edge	86
4.6c	A circle is constructed with IP as centre	87
4.6d	A triangular element is constructed by having IP as the vertex	87
4.7a	No object lies within the circle	88
4.7b	An equilateral triangle is constructed	88
4.8a	Two types of the object lie within the circle which are active nodes and active edges	89
4.8b	Node d is selected as the vertex	89
4.9a	An active edge intersected with the circle with $L_{bp1} < r$	90
4.9b	The IP becomes node d , the new active node for the triangular element	90
4.10a	The intersected active edge is (b,c) with $L_{bp1} \geq r$	91
4.10b	The triangular element is constructed by connecting the node associated with the intersected active edge to the base edge	91
4.11a	Two active edges with equal length to the radius intersected with the circle and at the same time all the nodes of the active edges are at the circum circle	92
4.11b	Three equilateral triangle elements are constructed simultaneously	92
4.12a	The base edge considered is (a,b) and its IP for example 1	93
4.12b	Position the crosshair until a small purple colored circle appears at IP	94
4.12c	The crosshair is moved towards either node of the base edge until a small purple colored circle appears at the respective node	95

4.12d	A circle with its centre at IP and $r = L_{base_edge}$ is automatically created	95
4.12e	An equilateral triangle is constructed for example 1	96
4.13a	A circle with its centre at IP and $r = L_{base_edge}$ is constructed for example 2	97
4.13b	Among the process to creating the temporary line from node d to IP	98
4.13c	The distance between node d and IP is 0.2604	99
4.13d	The distance between node c and IP is 0.5049	99
4.13e	Node d is selected as a vertex for example 2	100
4.14a	A circle with its centre at IP and $r = L_{base_edge}$ is constructed for example 4	101
4.14b	Creating the intersection point $p1$	102
4.14c	A temporary line to determine the distance L_{bp1}	102
4.14d	An equilateral triangle is created when IP is selected as the vertex for example 4	103
4.15a	A circle with its centre at IP and $r = L_{base_edge}$ is constructed for example 5	104
4.15b	A temporary line to determine the distance L_{bp1}	105
4.15c	Node c is selected to be the vertex of the new triangular element for example 5	105
4.16a	A circle with its centre at IP and $r = L_{base_edge}$ is constructed for example 6	106
4.16b	One of the new edges that need to be created by connecting node e to the node that lie at the circum circle	107
4.16c	Three equilateral triangles are constructed for example 6	107
4.17a	The initial front	111
4.17b	The first triangular element creation in the front	111

4.17c	The second triangular element creation in the front	111
4.17d	The third triangular element creation in the front	111
4.17e	The entire active edges of the first or initial front has been completely triangulated and form the second front	112
4.17f	The entire active edges of the second front has been completely triangulated and form the third front	112
4.17g	The entire active edge of the third front has been triangulated	113
4.17h	Triangular element mesh in the sub-region	113
4.18	EAFT-2 without the layer concept for domains with one circle	120
4.19	EAFT-2 incorporating the layer concept for domains with one circle	120
4.20a	Element with quality $Q_{EAS} = 0$	121
4.20b	Element with quality $0 < Q_{EAS} \leq 0.25$	121
4.20c	Element with quality $0.25 < Q_{EAS} \leq 0.5$	122
4.20d	Element with quality $0.5 < Q_{EAS} \leq 0.75$	122
4.21	EAFT-2 incorporating the layer concept for domains with two circles representing one complete reactor coil	123
4.22a	Element with quality $Q_{EAS} = 0$	124
4.22b	Element with quality $0.25 < Q_{EAS} \leq 0.5$	124
4.22c	Element with quality $0.5 < Q_{EAS} \leq 0.75$	124
4.23	The plot of convergence for simplified conceptual model with one circle	125
4.24	The plot of convergence for simplified conceptual model with two circle	126
4.25	The contour of temperature (K) distribution of the flue gas for the domain with 1 circle	127
4.26	The contour of temperature (K) distribution of the flue gas for the domain with two circles (one complete reactor coil)	127

4.27	The flue gas temperature (K) profile along the width of the furnace with one circle at $y=1.5$	128
4.28	The flue gas temperature (K) profile along the width of the furnace with two circles (one complete reactor coil) at $y=1.5$	128
5.1	The top view of the furnace taken from [33] with sensors placed along the wall	131
5.2a	Definition of boundary edges at boundary curves	132
5.2b	The whole domain is divided into sub-regions	132
5.3	Applying the layer concept at the newly created line segment (the newly created boundary of the sub-regions - AB and BC)	133
5.4a	The base edge is (11,12). Intersection point of the two circles is the IP	134
5.4b	IP on the perpendicular bisector of the base edge	134
5.4c	A circle is constructed with IP as centre	135
5.4d	A triangular element is constructed by having IP as the node	135
5.5a	No object lies within the circle	136
5.5b	An equilateral triangle is constructed	136
5.6a	Two types of the object lie within the circle which are active nodes and active edges	136
5.6b	Triangular element is constructed with edge (b,d)	136
5.7a	An active edge intersected with the circle	137
5.7b	The IP becomes the new active node for the triangular element	137
5.8a	The intersected active edge is (b,c) . The length of intersection point $p1$ and $p2$ with the circle is more than the length of the radius and at the same time $L_{ie} < 2 * L_{base_edge}$	138
5.8b	The triangular element is constructed by connecting the node associated with the intersected active edge with the base edge	138
5.9a	The intersected active edge is (b,c) . The three conditions which are $L_{p1p2} \geq r$, $L_{(b,c)} \geq 2 * L_{(a,b)}$ and $\frac{L_p}{L_{(b,c)}} < 0.1$ are satisfied.	139

- 5.9b The triangular element is constructed by connecting the node associated with the intersected active edge to the base edge 139
- 5.10a The intersected active edge is (b,c) . The three conditions, $L_{p1p2} \geq r$, $L_{(b,c)} \geq 2 * L_{(a,b)}$ and $\frac{L_p}{L_{(b,c)}} \geq 0.1$ are satisfied. 140
- 5.10b The triangular element is constructed by connecting the node associated with the intersected active edge to the base edge. 140
- 5.11a The base edge considered is (a,b) and its IP for example 1 141
- 5.11b The crosshair is first positioned at IP and left click on it when a small purple colored circle appears at IP 142
- 5.11c The crosshair is moved towards either of the nodes of the base edge until a small purple colored circle appears at the respective node 143
- 5.11d A circle is automatically created 143
- 5.11e Left click on the circum circle and delete the existed radius value in the properties window 144
- 5.11f A circle with its centre at IP and $r = 0.0679$ is created 144
- 5.11g An equilateral triangle is constructed for example 1 145
- 5.12a A circle with its centre at IP and $r = 0.0549$ is constructed for example 2 146
- 5.12b The new triangular element is a combination of edge (a,b) , (b,c) and (a,c) as the three sides of the triangle for example 2 147
- 5.13a A circle with its centre at IP and $r = 0.8 * L_{base_edge}$ is constructed for example 3 148
- 5.13b Edge (b,c) intersects with the circle with its length is $L_{ie} = 0.75$ 149
- 5.13c The intersection points are created and $L_{p1p2} \geq r$ 149
- 5.13d Node c is selected to be the vertex to form the triangle element for example 3 150
- 5.14a The base edge considered is (a,b) for example 4 151

- 5.14b The three edges (b,c) , (b,d) and (c,d) are connected to themselves and they become the sides of the second triangular element automatically 151
- 5.15a The base edge considered is (a,b) for example 5 152
- 5.15b Edge (a,c) intersects with the circle with its length is $L_{ie} = 0.7202$ 153
- 5.15c The intersection points are created and its distance is $L_{p1p2} \geq r$ 154
- 5.15d The crosshair is moved towards the intersected active edge until a small purple colored symbol of perpendicular appears at the intersected active edge 154
- 5.15e The perpendicular line of the intersected active edge connecting to the IP is then created with $L_p = 0.1451$ 155
- 5.15f The first element is created when the nodes of the base edge are connected to node d 155
- 5.15g The second element is created when the node of the active edge of (a,c) is connected to node d 156
- 5.16a A circle with its centre at IP and $r = 0.8 * L_{base_edge}$ is constructed 157
- 5.16b The intersection points are created and $L_{p1p2} < r$ 158
- 5.16c A triangular element is constructed with edges (a,b) , (a,d) and (b,d) as the three sides of the triangular element for example 6 158
- 5.17a A circle with its centre at IP and $r = 0.8 * L_{base_edge}$ is constructed for example 7 159
- 5.17b The edge (a,c) intersects with the circle with its length is $L_{ie} = 0.5891$ 160
- 5.17c The intersection points are created and its distance is $L_{p1p2} \geq r$ 161
- 5.17d The perpendicular line is created and its length is $L_p = 0.0537$ 161
- 5.17e Node c which is the node associated with active edge (a,c) is selected to be the vertex to form the triangle element 162

5.18a	The initial or first front	165
5.18b	The first and second triangular element creation in the front	165
5.18c	The third and fourth triangular element creation in the front	166
5.18d	All the active edges of the departure zone group of the initial front become passive and form the second front	166
5.18e	All the active edges of the departure zone group of second front become passive and form the third front	167
5.18f	All the active edges of the departure zone group of the third front become passive and form the fourth front	167
5.18g	All the active edges of the departure zone group of fourth front become passive and form the fifth front	167
5.18h	Triangular element mesh in the sub-region	167
5.19a	ABE and BCE are poor elements	170
5.19b	Adjacent element is subdivided at the centroid	170
5.19c	A new polygon is formed when the poor elements and the newly developed element which share the same edge with the poor elements are deleted	171
5.19d	New elements are created when the polygon is subdivided at the centroid	171
5.20	The resulting initial mesh using the algorithm of EAFT-3 for conceptual model of ethylene furnace	174
5.21a	Zoom of the initial unstructured triangular elements at the inlet reactor	175
5.21b	Zoom of the initial unstructured triangular elements at the outer reactor coils	175
5.22a	Element with quality $Q_{EAS} = 0$	176
5.22b	Element with quality $0 < Q_{EAS} \leq 0.25$	176
5.22c	Element with quality $0.25 < Q_{EAS} \leq 0.5$	176
5.22d	Element with quality $0.5 < Q_{EAS} \leq 0.75$	176

5.22e	Element with quality $0.75 < Q_{EAS} \leq 0.9$	176
5.22f	Element with quality $0.9 < Q_{EAS} \leq 1$	176
5.23	The resulting initial unstructured mesh with SAFT algorithm for conceptual model of furnace	178
5.24	The resulting final mesh for the conceptual model with EAFT-3 after the post-processing procedure	179
5.25a	Element with quality $Q_{EAS} = 0$	180
5.25b	Element with quality $0 < Q_{EAS} \leq 0.25$	180
5.25c	Element with quality $0.25 < Q_{EAS} \leq 0.5$	180
5.25d	Element with quality $0.5 < Q_{EAS} \leq 0.75$	180
5.26	The resulting initial unstructured mesh using the algorithm of EAFT-3 for the simplified conceptual model as in Figure 4.1a	181
5.27	The plot for convergence	182
5.28	The contour of the flue gas temperature in the furnace	183
5.29a	Circumferential heat flux distribution (Wm^{-2})	184
5.29b	Circumferential reactor coil skin temperature (K)	184
6.1	The contribution of the study in the area of unstructured mesh is shaded with gray color	188
6.2	The comparative progressive between all the versions of the EAFT	189

LIST OF SYMBOLS / NOTATIONS

Roman Letters

a, b, c, d, e	-	nodes considered for element creation procedure
A, B, C, D	-	node forming the background grid
A_i	-	i th surface area
$b_{n,n+1}$	-	distance of the potential point from the edge which join node n and $n + 1$
c	-	intersection with y -axis
d_i	-	layer
D_i	-	the product of the normal unit vector at the i th surface and the intensity direction Ω^m
E	-	emissive power
E_b	-	emissive power of blackbody
E_s	-	emissive power of real surface
$Edge_sensor_i$	-	sensor boundary edge
i	-	node
$i\ dim$	-	dimensionality of the problem domain
IP	-	ideal point
K	-	number of pivot point
I	-	radiation intensity
I_b	-	radiation intensity of blackbody
I_s	-	radiation intensity of real surface
I^m	-	intensity along direction Ω^m

$I^{m'}$	-	intensity along direction $\Omega^{m'}$
$I_{P_i}^m$	-	intensity at cell P_i
l	-	length of the selected shortest active edge
L	-	total length of the straight line
L_{bp1}	-	length between the connected node of the base edge and intersection point $p1$
Ld_i	-	Length of the layer
L_{base_edge}	-	length of the base edge
L_{ie}	-	the whole length of the intersected active edge
L_p	-	the length of the perpendicular line of the intersected active edge connecting directly to the IP
L_{p1p2}	-	length between the intersection points
m	-	number of layer
m_{ie}	-	the slope of intersected active edge
M	-	total number of discrete directions
M	-	number of sub-regions
n	-	node
n	-	total number of edges from the layer concept
n_s	-	number of nodes adjacent to node i
\mathbf{n}	-	outward surface normal
N_i	-	outer boundary nodes
p	-	centre of local umbrella
p	-	total number of inner boundary edges in the whole domain
p_s, p_e	-	point at local umbrella
p^1, p^2	-	intersection points of the active edge and circle
P_i	-	neighbour cell of cell P with i th surface as the same face between P and P_i
q	-	heat flux

q	-	total number of outer boundary edges in the whole domain
Q_{EAS}	-	EquiAngle Skew
Q_{EVS}	-	EquiSize Skew
r	-	radius of the circle for triangular element creation
r_j	-	reference number for inner boundary edge
r_k	-	reference number for outer boundary edge
r_l	-	reference number for edges from layer concept
r_t	-	reference number for new edge created in the whole domain
\mathbf{r}	-	position vector
\mathbf{r}_w	-	position vector for a point on a diffusively emitting and reflecting gray surface
N_n	-	optimal number of new points
N_p	-	total surface number for cell P
S	-	stretching parameter
S	-	area of the mesh elements
S_{eq}	-	maximum area of the equilateral triangle circumscribing radius of which is identical to that of the mesh element
T	-	absolute temperature
T_i	-	temperature obtained from the sensor at outer boundary node
$T_{Edge_sensor_i}$	-	average temperature value of sensor boundary edge
$w^{m'}$	-	solid angle associated with direction $\Omega^{m'}$
x_j	-	x coordinate of the neighbouring node with reference number j
y_j	-	y coordinate of the neighbouring node with the reference number j
(x_a, y_a)	-	the co-ordinate of node a
(x_b, y_b)	-	the co-ordinate of node b

(x_c, y_c)	-	the co-ordinate of active node c
(h, k)	-	The co-ordinate of IP
(x_{p1}, y_{p1})	-	the co-ordinate of intersection point $p1$
(x_{p2}, y_{p2})	-	the co-ordinate of intersection point $p2$
(x_p, y_p)	-	the co-ordinate of the point where both of the perpendicular line and the intersected active edge cross

Greek Letters

α_n	-	angle between edges
δ	-	size parameter of the mesh
$\delta_{n-1,n}, \delta_{n,n+1}$	-	length of adjacent edge
ϕ	-	orientation of the cells
σ	-	Stefan-Boltzmann's constant
σ_s	-	scattering coefficient
ε	-	surface emissivity
κ	-	absorption coefficient
β	-	extinction coefficient
Ω	-	direction of intensity
$\Phi(\Omega' \rightarrow \Omega)$	-	scattering phase function from the incoming direction, Ω' to the outgoing direction, Ω
Ω^+	-	leaving radiation intensity direction
Ω^-	-	arriving radiation intensity directions
Ω^m	-	discrete direction of radiation intensity
μ	-	cosines of direction along the Cartesian co-ordinate x
η	-	cosines of direction along the Cartesian co-ordinate y

ξ	-	cosines of direction along the Cartesian co-ordinate z
ΔV_p	-	the volume of cell P
θ_{max}	-	maximum angle between edges
θ_{min}	-	minimum angle between edges
θ_{eq}	-	characteristic angle corresponding to an equilateral element

CHAPTER 1

INTRODUCTION

1.1 Research background

Ethylene is the greatest olefin market where most of it is consumed in plastic production [1]. 90% of ethylene in the Europe is produced from steam cracking using naphtha as the feedstocks while in North America and Middle East use ethane and propane as the feedstocks [2]. Ethylene is an important chemical compound produced in the petrochemical industry and is produced from the steam cracking process in ethylene cracker furnaces [3, 4]. In steam cracking, heat is used for breaking or cracking down the saturated hydrocarbon or feedstocks into smaller hydrocarbon in the reactor coils or reactor tubes, which eventually produces the desired products such as ethylene.

Of all the heat transfer modes, radiation plays a significant role in the ethylene production [5-10]. It has been noted in [6, 11] that more than 90% of the heat transfers in the ethylene furnace involve radiation. Radiation is caused by energy emission in the form of electromagnetic waves or streams of photons [12]. The heating process in the ethylene furnace begins when burners which are located on the floor near the furnace wall heat up the furnace. This happens because the combustion process carried out in the burner resulted in flames and the release of its hot flue gas. These flue gas are composed of carbon dioxide, water vapour, oxygen and nitrogen [13]. The radiative heat from the furnace wall and hot flue gas is then transferred to reactor tubes/coils.

The desired parameters of the heat transfer in ethylene furnace study are the temperature and the radiative heat flux. In order to obtain such parameters, the whole process of the fluid flow simulation in Computational Fluid Dynamics (CFD) need to be done where it involves all three elements namely pre-processing, solving and the post-processing. As a matter of fact, structured or unstructured triangular mesh formation fall into the pre-processing element in CFD [14]. The generation of triangular mesh is an important step for approximating solutions to boundary value problems. Among the two type of meshes, unstructured mesh are becoming predominant because of its ability of modeling complex geometry as well as the natural environment it has for adaptivity [15, 16].

There are two basic approaches for unstructured mesh namely the Delaunay triangulation and the advancing front technique. The Delaunay triangulation is a method of generating elements by adding or inserting points in the interior and reconnecting it to form the element [15, 17-21]. The insertion of the points can be controlled by several methods reported in [22]. On the other hand, the advancing front technique generate element with its key algorithmic step is the appropriate introduction of the new elements to the empty region [19, 21, 23]. It must be noted that the elements and the nodes in this technique are placed simultaneously in the region [24].

The advancing front technique places a new element by considering an ideal point generated as well as the existing nodes in the circle constructed. The centre of the circle is the ideal point and the radius is calculated based on the empirical rules for the element creation procedure. The advancing front technique is guaranteed to preserve boundary integrity as well as having the capacity to create triangular elements with high aspect ratios in the boundary-layer region [15, 25]. However, there are also method of combining the approach of Delaunay and advancing front techniques for generating unstructured mesh such as in [25-31].

In [32], the author highlighted three cases as being possible during the procedure of element creation with the approach of advancing front technique:

- (1) A new element is created with a new node as a vertex in which the new node is joined to the edge being considered.
- (2) An already existing front node satisfying certain conditions in the proximity of the edge being considered is used to create a new element.
- (3) Neither of the cases above in which an efficient algorithm of mesh generation should be able to tackle such a problem.

With the advancing front technique as the approach for triangulation in the study, it can be seen that there is an improvement that need to be done towards the algorithm. The new improved algorithm of advancing front technique will be used to generate the unstructured meshes in the computational domain of the ethylene furnace for further modeling and simulation work.

1.2 Problem statement

The limitation of the current practice of monitoring and measuring the radiative heat transfer in ethylene furnace is addressed in this research. Furthermore, the current practice of the iterative approach in both finite volume and finite element also assume the initial intensity value to be zero because of unknown temperature distribution in the ethylene furnace. Hence, in this study a number of problems are addressed:

- 1) Given a set of sensors distributed along the wall of the ethylene furnace, in what way can the domain be partitioned into meshes in the form of triangle so as to support approximation of the temperature of the flue gas and the radiative heat flux distribution inside the furnace using methods like discrete ordinate, finite volume and etc?
- 2) What are the algorithms for effectively generating initial unstructured mesh that is appropriate for the conceptual model of integrating sensor network with the radiative heat transfer equation in ethylene furnace? The algorithm of the unstructured mesh must be able to tackle the problem of invalid or

undecided element creation in the algorithm.

- 3) What is the appropriate mesh post-processing procedure to improve the quality of the initial unstructured mesh if required?

1.3 Objectives and scope of the research

The objectives of the research are as follows:

- Objective 1: To study the phenomena of heat transfer process in ethylene furnace and the current practice of monitoring the temperature and radiative heat flux.
- Objective 2: To develop a conceptual model of integrating sensor network and radiative heat transfer equation in ethylene furnace.
- Objective 3: To develop new algorithms for the initial unstructured grid that is appropriate for the conceptual model of integrating sensor network and radiative heat transfer equation in ethylene furnace.
- Objective 4: To perform simulations using discrete ordinate method on the newly developed unstructured grid in order to obtain the smooth distribution of the flue gas temperature and radiative heat flux in the ethylene furnace.

The research concentrates on developing algorithm of initial unstructured triangular mesh for element creation procedure following the approach of advancing front technique in two dimensional domains. The research focused on triangular element since it is reported in [15, 16] that this element are the most flexible for complex two dimensional geometries especially when grading of the mesh is required. Although there are many more models in the ethylene furnace study, only radiation model will be considered for the present research. Therefore, the algorithm of unstructured mesh will be applied in the conceptual model of integrating sensor network and radiative heat transfer in order to obtain flue gas temperature and radiative heat flux in the ethylene furnace.

1.4 Research methodology

The methodologies in the research involve the following steps:

(1) Literature review

The ethylene furnace design, process descriptions, problem related to ethylene furnace, current techniques of modeling and simulating the ethylene furnace, the unstructured mesh formation and the discretisation technique as well as the type of temperature sensor will be studied through books, journal papers and conference proceedings. This first step is very helpful in order to obtain a wider view on the whole problem domain.

(2) Analysis phase

The furnace designs, the processes involved in the furnace as well as the selected problems are carefully analyzed. This is associated with the current methods and techniques of solving the furnace model with special attention to radiation model. At the same time, the basic concepts of advancing front techniques together with its recent approaches are analyzed for the conceptual model in the research. The analysis of the unstructured mesh is done through studying and applying the standard algorithm in both simple and complex computational domain in order to figure out any space for improvement. The current problems of undecided element creation are spotted when the algorithm of standard advancing front techniques are implemented in AutoCAD software to discretise several domains of the study.

(3) Design phase

A few versions of the algorithm of enhanced advancing front technique with a set of structured cases for element creation procedure are designed and developed to encounter the existing problem as stated in the last two paragraphs of Section 1.1. At the same time, the conceptual model of integrating sensors and unstructured mesh with radiative heat transfer equation in the furnace is designed. In the conceptual model, sensors are assumed to be placed along the wall of the furnace in order to

obtain boundary value for the radiative heat transfer model. The research focused on two dimensional model and therefore a cross section of the furnace is considered for the conceptual model.

(4) Implementation phase

As stated in Section 1.1, the CFD simulation involves three elements. The first element which is the pre-processing in this study involves the definition of the geometry of the ethylene furnace as the computational domain, mesh formation and the selection of physical phenomena that need to be modelled. In this study, the pre-processing element belongs to the implementation phase. The geometry of the ethylene furnace follows the one in the literature survey. The major contribution of the study focus on unstructured mesh, therefore, various simulation of the newly developed algorithm for the initial unstructured mesh is conducted and implemented in AutoCAD LT software. The selection of the physical phenomena of heat transfer as well as the fluid properties follows the existing research in ethylene furnace study.

(5) Testing and evaluation phase

As for testing and evaluation phase, the quality of the initial mesh implemented in the previous phase is determined using a number of measurements in GAMBIT 3.0 software. The mesh post-processing procedure is applied where required. The second element in CFD which is the solving process belongs to the testing and evaluation phase in the study. It involves numerical solution techniques using FLUENT software. As a matter of fact, this is one of the methods that can be considered to test and prove that the resulted unstructured mesh for the conceptual model is appropriate for further analysis. FLUENT is used to integrate and solves the governing equation of the heat transfer over all the unstructured mesh developed which represents the ethylene furnace. The discretisation technique of discrete ordinate method is used to convert the governing equation into a set of a system of algebraic equations. An iterative method is used to solve algebraic equations. The third element in CFD which is the post-processing also belongs to the testing and evaluation phase in the study. It involves the data visualisation for the final results. The results of the study are displayed as the contour of the flue gas temperature

distribution. Besides that, the circumferential radiative heat flux and the circumferential temperature of the reactor coils are also obtained and displayed in the study.

(6) Documentation

The work is reported in this thesis. The report presents all the concepts, simulation work, its analysis and results throughout the research.

The framework of the research is summarised in Figure 1.1a and Figure 1.1b.

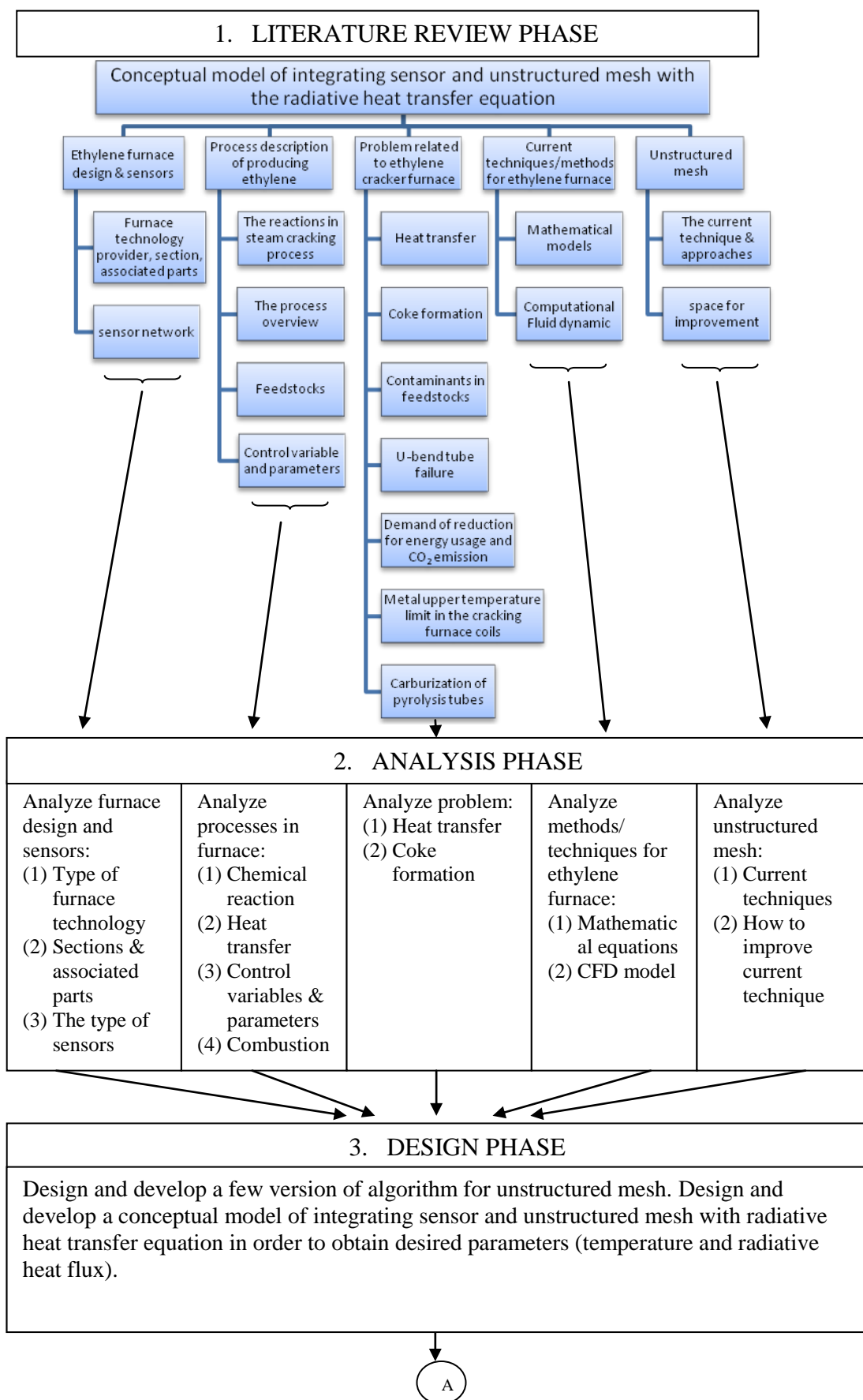


Figure 1.1a. The framework of the research – part 1.

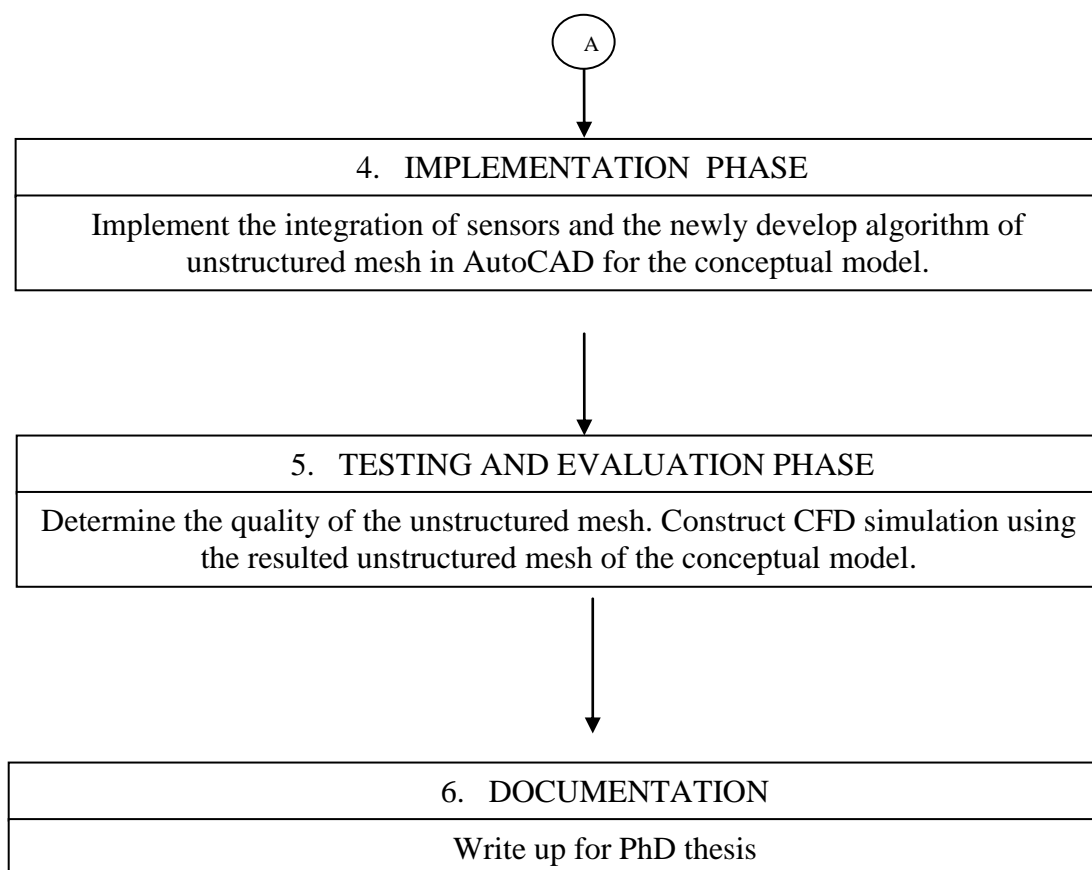


Figure 1.1b. The framework of the research – part 2.

1.5 Significance of the research

This research will contribute in improving the approach of modeling and simulation study in an ethylene furnace where most of the current techniques use only existing mesh generation software (GAMBIT etc) and CFD solver software (FLUENT, SPYRO etc) to predict the performance and behavior of operating parameters in the furnace operations. Since temperature plays a significant role in the daily operation of the ethylene furnace, it is of great importance to monitor the flue gas temperature distribution in the furnace, the radiative heat flux as well as the temperature of the reactor coils. This proactive approach of coupling a set of sensors in the furnace environment will provide continuous monitoring for further action to the furnace operator and engineers.

Therefore, a conceptual model of integrating sensor network and radiative heat transfer in the ethylene furnace environment is crucial as an initial phase of incorporating the ideas to the real world application. Sensors will be used to provide input in the form of boundary values for the simulation. Furthermore, the framework of the conceptual model provides the algorithm of initial triangular unstructured mesh where it incorporates the sensors deployment and a way of gradual mesh control. Besides that, it must be noted that the algorithm of the initial unstructured mesh is capable of constructing the triangular element directly in every iteration without having to re-order the front or delete the existing element as highlighted in the literature.

1.6 Outline of the thesis

An overview of the whole research is presented in Chapter 1 of the thesis. The research background of the ethylene furnace as well as the existing method of unstructured mesh formation is briefly described in the early part of the chapter. This is continued with the problem statements, the objectives and scope of the research as well as the research methodology and the significance of the research. The literature review is presented in Chapter 2 while a few versions of the unstructured mesh algorithm are developed and discussed from Chapter 3 through Chapter 5.

The discussion in Chapter 2 begins with an overview of ethylene furnace and its processes. This is followed by the phenomena of heat transfer in ethylene furnace and the current technique of monitoring heat transfer parameter where it serves as a foundation for setting up the conceptual model. The main contribution of the research is on the algorithm of unstructured mesh formation therefore an overview of related existing techniques of Delaunay mesh triangulation and advancing front techniques are discussed. This is followed by the existing mesh post-processing procedure for improving the quality of the mesh. The newly developed mesh is applied to solve the problem of radiation in the ethylene furnace, therefore the concept of radiation together with the Discrete Ordinate methods (DOM) as the

discretisation techniques are also described. At the end of the chapter, a review of the types of temperature sensors is presented.

Chapter 3 addressed the current problems in the element creation procedure of the standard advancing front technique. This problem has become a motivational reason of the need to enhance the current techniques in terms of element creation procedure. The first version of the newly developed algorithm for the unstructured mesh in this research is called as Enhanced Advancing Front Technique-1 (EAFT-1). The creation of the element in EAFT-1 is based on the five structured cases whereas the original technique has only two cases. The EAFT-1 is applied at a simple problem with enclosed wall where there is no inner boundary. The resulted unstructured mesh from the algorithm of EAFT-1 is integrated with the radiation model in order to prove that the mesh is appropriate for further analysis.

The second version of the unstructured mesh in Chapter 4 is called as Enhanced Advancing Front Technique-2 (EAFT-2). The element creation procedure in EAFT-2 is based on six structured cases. The radius of the circle during the element creation procedure does not follow the empirical rule as in SAFT but instead it is simpler than that. The departure zone for the element creation is set to be the entire front starting with the shortest edge. The algorithm of EAFT-2 incorporates the sensors as the boundary nodes forming boundary element. In order to tolerate the smaller size of element span over the shortest edges and the bigger size of the boundary element, the layer concept is introduced for internal gradation control of the mesh size. The EAFT-2 is applied at two simple conceptual models where in both conceptual model, the sensors are assumed to be placed along the wall. At the same time, the numbers of reactor coils in both simple conceptual models are reduced to only one complete reactor coil and half of the complete one reactor coil respectively.

The third version of the unstructured mesh in Chapter 5 is called as Enhanced Advancing Front Technique-3 (EAFT-3). The element creation procedure in EAFT-3 is based on seven structured cases. The radius of the circle during the element creation procedure in EAFT-3 is set to be eighty percent from the length of the base

edge. The departure zone for the element creation is set to be the specific front starting with the shortest edge. Similar to the approach introduced in Chapter 4, the layer concept is used for mesh size internal gradation control. A newly developed post-processing procedure to improve the quality of the mesh is also introduced in which it is called as EAFT-3 polygon refinement procedure. The algorithm of EAFT-3 is applied to the conceptual model which is designed and developed for ethylene furnace. The configuration of the ethylene furnace for the conceptual model followed the one in [33] and it is assumed that there is a set of sensors placed along the wall. The function of the sensors is to provide valuable input in the form of boundary value. At the end of the chapter, the resulted unstructured mesh incorporated with the conceptual model is applied for radiation problem in FLUENT software. The simulation converged and the desired parameters such as the flue gas temperature distribution, circumferential radiative heat flux and the circumferential skin temperature at the reactor coils are obtained.

The summary for every version of enhanced advancing front techniques can be found in Chapter 6. This final chapter also contains the contributions of the research in the aspect of unstructured mesh which are presented at the end of the chapter.

REFERENCES

1. Hensman, A., *Focus on ethylene*, in *Chemical week*. 2009, ProQuest Central. p. S3.
2. Burrige, E., *Ethylene*, in *European Chemical News*. 2005, ProQuest Central. p. 26.
3. Gielen, D., K. Bennaceur, and C. Tam, *IEA Petrochemical Scenarios for 2030-2050: Energy Technology Perspectives*, in *International Workshop on Technology Learning and Deployment*. 2007, IEA: Paris.
4. Picciotti, M., *Novel ethylene technologies developing but steam cracking remains king*. *Oil & Gas Journal*, 1997. **95**(25).
5. Han, Y., R. Xiao, and M. Zhang, *Combustion and Pyrolysis Reactions in a Naphtha Cracking Furnace*. *Chemical Engineering & Technology*, 2006. **30**(1): p. 112-120.
6. Guihua, H., W. Honggang, and Q. Feng, *Numerical simulation on flow, combustion and heat transfer of ethylene cracking furnaces*. *Chemical engineering science*, 2011. **66**(8): p. 1600-1611.
7. Habibi, A., B. Merci, and G.J. Heynderickx, *Impact of radiation models simulations of steam cracking furnaces*. *Computer and Chemical Engineering* 2007. **31**: p. 1389-1406.
8. Nouwen, W., et al., *Simulation tools evaluate large-capacity furnace designs*. *Oil & Gas Journal*, 1998. **96**(12).
9. Cremer, M., et al. *Improving the performance of process heaters through fireside modeling*. in *AFRC International Symposium*. 1997. Chicago.
10. Aminian, J., S. Shahhosseini, and M. Bayat, *Investigation of temperature and flow Fields in an Alternative Design of Industrial Cracking Furnaces Using CFD*. *Iranian Journal of Chemical Engineering*, 2010. **7**(3): p. 61-73.
11. Heynderickx, G.J. and M. Nozawa, *High-emissivity Coatings on Reactor Tubes and Furnace Walls in Steam Cracking Furnaces*. *Chemical Engineering Science*, 2004. **59**: p. 5657-5662.
12. Modest, M.F., *Radiative Heat Transfer*. 2 ed. 2003: Academic Press. 822.
13. Stefanidis, G., et al., *Gray/nongray gas radiation modeling in steam cracker CFD calculations*. *AIChE Journal*, 2007. **53**(7): p. 1658–1669.
14. Koomullil, R., B. Soni, and R. Singh, *A comprehensive generalized mesh system for CFD applications*. *Mathematics and Computers in Simulation*, 2008. **78**: p. 605-617.
15. Farrashkhalvat, M. and J.P. Miles, *Basic structured grid generation with an introduction to unstructured grid generation*. 2003: Butterworth Heinemann.
16. Lyra, P.R.M. and D.K. Carvalho, *A computational methodology for automatic two-dimensional anisotropic mesh generation and adaptation*. *Journal of the Brazilian Society of Mechanical Sciences and Engineering*, 2006. **28**(4): p. 399-412.

17. Rebay, S., *Efficient unstructured mesh generation by means of delaunay triangulation and Bowyer-Watson algorithm*. Journal of Computational Physics, 1993. **106**(1): p. 125-138.
18. Teng, S.-H. and C.W. Wong, *Unstructured mesh generation: Theory, practice and perspectives*. International Journal of Computational Geometry and Applications, 2000. **10**(3): p. 227-266.
19. Lohner, R., *Progress in Grid Generation via the Advancing Front Technique*. Engineering with Computers, 1996: p. 186-210.
20. Mavriplis, D.J., *Unstructured grid technique*. Annual Review Fluid Mechanics, 1997: p. 473-514.
21. Bathe, K.-J., *Current directions in meshing*, in *Mechanical Engineering*. 1998, ProQuest Central.
22. Muylle, J., P. Ivanyi, and B.H.V. Topping, *A new point creation scheme for uniform Delaunay triangulation*. Engineering Computations, 2002. **19**: p. 707-735.
23. Liseikin, V.D., *Unstructured Methods*, in *Grid Generation Methods*. 2010, Springer
24. Cebeci, T., et al., *Grid Generation*, in *Computational Fluid Dynamics for Engineers*. 2005, Springer Berlin Heidelberg. p. 263-294.
25. El-Hamalawi, A., *A 2D combined advancing front-Delaunay mesh generation scheme*. Finite elements in analysis and design, 2004. **40**: p. 967-989.
26. Muller, J.D., P.L. Roe, and H. Deconinck, *A frontal approach for internal node generation in delaunay triangulations*. International Journal for Numerical Methods in Fluids, 1993. **17**: p. 241-255.
27. Mavriplis, D.J., *An Advancing Front Delaunay Triangulation Algorithm Designed for Robustness*. Journal of Computational Physics, 1995. **117**(1): p. 90-101.
28. Mavriplis, D.J., *Unstructured mesh generation and adaptivity*. 1995, Institute for Computer Applications in Science and Engineering (ICASE).
29. Frey, P.J., H. Borouchaki, and P.-L. George, *3D Delaunay mesh generation coupled with an advancing-front approach*. Computer methods in applied mechanics and engineering, 1998. **157**: p. 115-131.
30. Radovitzky, R. and M. Ortiz, *Tetrahedral mesh generation based on node insertion in crystal lattice arrangements and advancing-front-Delaunay triangulation*. Computational Methods in Applied Mechanics and Engineering., 2000. **187**: p. 543-569.
31. Sahimi, M., et al., *Upscaled unstructured computational grids for efficient simulation of flow in fractured porous media*. Transport in Porous Media, 2010. **83**(1): p. 195-218.
32. Kovac, N., S. Gotovac, and D. Poljak, *A New Front Updating Solution Applied to Some Engineering Problems*. Archives of Computational Methods in Engineering, 2002. **9**: p. 43-75.
33. Lan, X., et al., *Numerical Simulation of Transfer and Reaction Processes in Ethylene Furnaces*. Chemical Engineering Research and Design, 2007. **85**(A12): p. 1565-1579.
34. Zimmermann, H. and R. Walzl, *Ethylene*. 2005, Linde AG.
35. Silva, I.C., et al., *Carburization of ethylene pyrolysis tubes determined by magnetic measurements and genetic algorithm*. Scripta Materialia, 2007. **56**: p. 317-320.

36. Heyndericks, G.J., G.G. Cornelis, and G.F. Froment, *Circumferential tube skin temperature profiles in thermal cracking coils*. *AIChE Journal*, 1992. **38**(12): p. 1905-1912.
37. Bockelie, M.J., et al. *Computational simulations of industrial furnaces*. in *International Symposium on Computational Technologies For Fluid/Thermal/Chemical System with Industrial Applications*. 1998. California, USA.
38. Hillewaert, L.P., J.L. Dierickx, and G.F. Froment, *Computer generation of reaction schemes and rate equation for thermal cracking*. *AIChE Journal*, 1988. **34**(1): p. 17-24.
39. Edwin, E.H. and J.G. Balchen, *Dynamic optimization and production planning of thermal cracking operation*. *Chemical Engineering Science*, 2001. **56**: p. 989-997.
40. Karimzadeh, R., H.R. Godini, and M. Ghashghaee, *Flowsheeting of steam cracking furnaces*. *Chemical Engineering Research and Design*, 2009. **87**: p. 36-46.
41. Masoumi, M.E., et al., *Simulation, optimization and control of a thermal cracking furnace*. *Energy*, 2006. **31**: p. 516-527.
42. Niaei, A., et al., *The combined simulation of heat transfer and pyrolysis reactions in industrial cracking furnaces*. *Applied Thermal Engineering*, 2004. **24**: p. 2251-2265.
43. Goethem, M.W.M.V., et al., *Towards synthesis of an optimal thermal cracking reactor*. *Chemical Engineering Research and Design*, 2008. **86**: p. 703-712.
44. Geem, K.M.V., M.F. Reyniers, and G.B. Marin, *Challenges of Modeling Steam Cracking of Heavy Feedstocks*. *Oil & Gas Science and Technology* 2008. **63**(1): p. 79-94.
45. Yu, S., *Modelling and Simulation of Hydrocarbon Cracking*, in *School of Engineering*. 2007, Cranfield University. p. 88.
46. Sadrameli, S.M. and A.E.S. Green, *Systematics and modeling representations of naphtha thermal cracking for olefin production*. *Journal of Analytical and Applied Pyrolysis*, 2005. **73**: p. 305-313.
47. Stefanidis, G.D., et al., *Evaluation of high-emissivity coatings in steam cracking furnaces using a non-grey gas radiation model*. *Chemical Engineering Journal*, 2008. **137**: p. 411-421.
48. E, J., et al., *CRACKER - A PC Based Simulator for Industrial Cracking Furnaces* *Computers and Chemical Engineering*, 2000. **24**: p. 1523-1528.
49. *Furnaces, Heaters and Incinerators*. [cited 2011; Available from: linde-engineering.com].
50. Stefanidis, G., et al., *CFD simulations of steam cracking furnaces using detailed combustion mechanisms*. *Computers & Chemical Engineering*, 2006. **30**(4): p. 635-649.
51. Heynderickx, G.J., et al., *Three-Dimensional Flow Patterns in Cracking Furnaces with Long-Flame Burners*. *AIChE Journal*, 2001. **Vol. 47, No. 2**: p. 388-400.
52. Brown, D.J., et al. *Fireside modeling in cracking furnaces*. in *AIChE 9th Annual Ethylene Producers Conference*. 1997. Houston, USA.
53. Tang, Q., et al. *Advanced CFD Tools for Modeling Lean Premixed Combustion in Ultra-Low NO_x Burners in Process Heaters*. in *AFRC-JFRC Joint International Symposium 2004*. 2004.

54. Rahman, N.S.A., et al., *The state of the art for ethylene cracking furnace modeling*. 2008, Universiti Teknologi Malaysia.
55. Li, C., et al., *Fluid dynamic numerical simulation coupled with heat transfer and reaction in the tubular reactor of industrial cracking furnaces*. International Journal for Numerical Methods in Fluids, 2009. **62**(4): p. 355-373.
56. Belohlav, Z., P. Zamostny, and T. Herink, *The kinetic model of thermal cracking for olefins production*. Chemical Engineering and Processing, 2003: p. 461-473.
57. Cai, H., A. Krzywicky, and M.C. Oballa, *Coke formation in steam crackers for ethylene production*. Chemical Engineering and Processing, 2002: p. 199–214.
58. Schools, E.M. and G.F. Froment, *Simulation of decoking of thermal cracking coils by steam/air-mixtures*. AIChE Journal, 1997. **43**(1): p. 118-126.
59. Guo, Z., Z. Fu, and S. Wang, *Sulfur distribution in coke and sulfur removal during pyrolysis*. Fuel Processing Technology, 2007. **88**: p. 935-941.
60. Hájeková, E., et al., *Coke Formation during copyrolysis of polyalkenes with naphtha*. Petroleum & Coal, 2008: p. 52-55.
61. Colannino, J., *Ethylene furnace heat flux correlations*. 2008.
62. Oprins, A.J.M. and G.J. Heynderickx, *Calculation of three-dimensional flow and pressure fields in cracking furnaces*. Chemical Engineering Science, 2003: p. 4883 – 4893.
63. Li, B.Q., *Discontinuous Finite Elements in Fluid Dynamics and Heat Transfer*. 2006, Germany: Springer-Verlag. 586.
64. Versteeg, H.K. and W. Malalasekera, *An Introduction to Computational Fluid Dynamics*. 2007, England: Pearson Education.
65. Owen, S.J. *A survey of Unstructured Mesh Generation Technology*. in *International Meshing Roundtable 1998*. Dearborn, Michigan
66. Blazek, J., *Principles of Grid Generation*, in *Computational Fluid Dynamics: Principle and Applications*. 2007.
67. Peraire, J., J. Peiro, and K. Morgan, *Advancing front grid generation*, in *Handbook of Grid Generation*, N.P. Weatherill, B.K. Soni, and J.F. Thompson, Editors. 1999, CRC Press LLC.
68. George, A.J., *Computer Implementation of the Finite Element Method*, in *Department of Computer Science*. 1971, Stanford University.
69. S.H.Lo, *A New Mesh Generation Scheme for Arbitrary Planar Domains*. International Journal for Numerical Methods in Engineering, 1985. **21**: p. 1403-1426.
70. Persson, P.-O., *Lecture 1 Computational Mesh Generation*. 2008, MIT.
71. Zhu, J., T. Blacker, and R. Smith, *Background overlay grid size functions*, in *Proceedings of the 11th international meshing roundtable*. 2002. p. 65–74.
72. Seveno, E. *Towards an adaptive advancing front method*. in *6th International Meshing Roundtable*. 1997.
73. Naji, H.S., *An improved advancing front algorithm for triangulating arbitrary two dimensional regions*. 2004.
74. Minyi, K., C. Jie, and J. Huazhong, *Research of Using Dynamic Programming in the Nodes Encoding Optimization*, in *International Conference on Information Engineering and Computer Science*, 2009. 2009.
75. Ito, Y., et al., *Parallel unstructured mesh generation by an advancing front method*. Mathematics and Computers in Simulation, 2007. **75**: p. 200-209.

76. Sazonov, I., et al., *A stitching method for the generation of unstructured meshes for use with co-volume solution techniques*. Computational Methods in Applied Mechanics and Engineering., 2006. **195**: p. 1826–1845.
77. Hernández-Mederos, V., P.L.d. Ángel, and J. Estrada-Sarlabous, *Isotropic umbrella based triangulation of regular parametric surfaces*. Numer Algor, 2008. **48**: p. 29–47.
78. Wang, W.X., C.Y. Ming, and S.H. Lo, *Generation of triangular mesh with specified size by circle packing*. Advances in Engineering Software, 2007. **38**: p. 133-142.
79. Owen, S.J. *An Introduction to Mesh Generation Algorithm*. in *14th International Meshing Roundtable*. 2005. San Diego, California, USA.
80. Okusanya, T.O., *An algorithm for parallel unstructured mesh generation and flow analysis*, in *Department of Aeronautics and Astronautics*. 1996, Massachusetts Institute of Technology. p. 119.
81. Tremel, U., et al., *Parallel generation of unstructured surface grids*. Engineering with Computers, 2005: p. 36-46.
82. Sorli, K., *A Review of Computational Strategies for Complex Geometry and Physics*. 2002, CFD Applied to Reactor ProcEss Technology.
83. George, P.L. and E. Seveno, *The advancing front mesh generation method revisited*. International Journal for Numerical Methods in Engineering, 1994. **37**: p. 3605-3619.
84. Vasiliauskiene, L. and R. Bausys, *Intelligent Initial Finite Element Mesh Generation for Solutions of 2D Problems*. INFORMATICA, 2002. **13**: p. 239–250.
85. Vasiliauskiene, L., *Adaptive finite element strategies for solution of two dimensional elasticity problems*, in *Technological Sciences, Mechanical Engineering*. 2006, VILNIUS GEDIMINAS TECHNICAL UNIVERSITY.
86. Chong, C.S., A. Senthil Kumar, and H.P. Lee, *Automatic mesh-healing technique for model repair and finite element model generation*. Finite elements in analysis and design, 2007. **43**(15): p. 1109-1119.
87. Schoberl, J., *NETGEN An advancing front 2D/3D - mesh generator based on abstract rules*. Computing and Visualization in Science, 1997: p. 41-52.
88. Liu, J., H.M. Shang, and Y.S. Chen, *Development of an unstructured radiation model applicable for two-dimensional planar, axisymmetric, and three-dimensional geometries*. Journal of Quantitative Spectroscopy & Radiative Transfer 2000. **66**: p. 17-33.
89. Li, B.Q., *Radiative Transfer in Participating Media*, in *Discontinuous Finite Elements in Fluid Dynamics and Heat Transfer*, K.-J. Bathe, Editor. 2006, 3: Germany.
90. Lacanette, K., *National Temperature Sensor Handbook*. 1997: National Semiconductor. 42.
91. Chen, J., X. Hu, and L. Xu, *A New Thermocouple Auto-Calibration System*, in *International Conference on Computer Science and Software Engineering*. 2008, IEEE.
92. Zhang, M., *Research and Implement of Thermocouple Sensor and Microcontroller Interface*. 2010, IEEE.
93. *Sensor Types and Principles of Operation*, Testemp Ltd.
94. *RTD Theory*, SensorTec Inc.
95. Dogan, I., *Chapter 4 - RTD Temperature Sensors*, in *Microcontroller Based Temperature Monitoring and Control*. 2002, Newnes: Oxford. p. 87-106.

96. Wobschall, D. and W.S. Poh, *A Smart RTD Temperature Sensor with a Prototype IEEE 1451.2 Internet Interface in Sensor for Industry Conference*. 2004, IEEE: New Orleans, Louisiana, USA.
97. Dogan, I., *Chapter 5 - Thermistor Temperature Sensors*, in *Microcontroller Based Temperature Monitoring and Control*. 2002, Newnes: Oxford. p. 107-127.
98. (2003) *Introduction to AutoCAD LT. Volume,*
99. *Gambit 2.3 Documentation - Gambit User Guide*. [cited 2010 25 November]; Available from:
<http://my.fit.edu/itresources/manuals/gambit2.3/help/index.htm>.
100. Wang, K., *Numerical modeling of nasal cavities and air flow simulation*, in *Graduate Faculty*. 2006, Auburn University. p. 146.